

Noise-color-induced quenching of fluctuations in a correlated spontaneous-emission laser model

R. G. K. Habiger and H. Risken

Abteilung für Theoretische Physik, Universität Ulm, D-7900 Ulm, Federal Republic of Germany

M. James* and Frank Moss

Department of Physics, University of Missouri at Saint Louis, Saint Louis, Missouri 63121

W. Schleich

*Max-Planck-Institut für Quantenoptik, D-8046 Garching bei München, Federal Republic of Germany
and Center for Advanced Studies and Department of Physics and Astronomy, University of New Mexico,
Albuquerque, New Mexico 87131*

(Received 23 October 1989)

We show via (1) an approximate, analytical technique, (2) a formally exact matrix continued-fraction analysis, and (3) an analog simulation of the classical Langevin equation of a correlated spontaneous-emission laser (CEL) that noise of nonzero correlation time leads to an enhancement of the characteristic CEL noise quenching.

I. INTRODUCTION

Quantum noise determines the ultimate accuracy of active interferometers in applications such as gravitational wave detection¹⁻³ or in a ring-laser gyroscope.^{4,5} This discovery has motivated the investigation of laser systems with reduced spontaneous-emission noise such as the correlated (spontaneous) emission laser (CEL).⁶⁻⁸ Under appropriate conditions⁵⁻⁷ the relative phase angle ϕ between two electromagnetic waves in a CEL can be freed completely from the effect of spontaneous-emission noise. This noise quenching can be related⁹ to the fact that the phase fluctuations in a CEL enter into the phase Langevin equation as multiplicative¹⁰ rather than additive noise as, for example, in the standard phase-locked laser.¹¹ Moreover, in a laser consisting of long-lived atoms, the spontaneous-emission noise is colored¹² instead of white.^{13,14} Noise quenching as a result of multiplicative noise⁹ and the role of noise color^{14,15} are the themes that provide the stimulus for the present study of the influence of noise color on the CEL noise quenching via the classical Langevin equation,¹⁶ derived in Ref. 9.

In this paper we do not intend to present a theory of the CEL with long-lived atoms. Rather, we pursue the following strategies: First, we perform an approximate analysis of the classical Langevin equation governing the phase difference ϕ by linearization within the physically relevant range of parameters. With the help of some standard techniques of noise theory,¹⁷ we find the (approximate) width $\sigma^2 = \langle \phi^2 \rangle - \langle \phi \rangle^2$ of the steady-state probability distribution $P_{SS} = P_{SS}(\phi)$ for the relative phase ϕ , to be reduced by a factor $(1 + \gamma\tau_c)^{-1}$ compared to the white-noise case. Here τ_c is the noise correlation time and $\gamma = (b^2 - a^2)^{1/2}$, where b and a denote the laser gain and the detuning between the two waves, respectively. Thus the CEL noise quenching is not only preserved in the case of colored noise but is even enhanced.¹⁸

Moreover, the multiplicative noise causes a noise-induced drift $\langle \Delta \rangle$, as well as a separation between the maximum ϕ_{\max} of the steady-state solution P_{SS} and $\langle \phi \rangle$, that is, a noise-induced asymmetry, $\delta \equiv \langle \phi \rangle - \phi_{\max}$, as discussed for the case of white noise in Ref. 9. We here show that for weak noise, that is, for $D/b \ll 1$, these white-noise results⁹ for $\langle \phi \rangle$ and for δ are both reduced by the factor $(1 + \gamma\tau_c)^{-1}$.

In the second approach, we express the steady-state solution of the corresponding Fokker-Planck equation in terms of infinite matrix continued fractions. In work^{18,19} related to the present one we have always cast the recurrence relation obtained from the relevant Fokker-Planck equation into a three-term vector-recurrence relation in the index m of the Hermite functions.¹⁴ The dimension of the matrices determines then the number n of Fourier coefficients taken into account in the numerical evaluation of P_{SS} . Due to the sharpness of the present distribution, however, many Fourier components are needed and hence the dimension of the matrices to be inverted has to be large in order to obtain convergence. It is therefore more convenient to use a new vector recurrence in n . In order to demonstrate this advantage, we compare and contrast the two methods by presenting the detailed equations. Moreover, we calculate the crucial quantities σ and δ confirming the noise-color-induced noise quenching found via the approximate Langevin treatment.

We conclude by simulating the Langevin equation of the CEL with an electronic circuit using a circuit and techniques similar to those previously described.¹⁹ The simulator provides immediately the steady-state distributions P_{SS} . We find qualitative agreement between the measured and calculated results and, in particular, we are able to confirm the predicted enhancement of the CEL noise quenching by color. Moreover, the analog simulation demonstrates another surprising effect caused by

multiplicative noise: a second maximum in P_{SS} , located approximately at the maximum of the potential V of the noise-free problem. The origin of this additional maximum is a time-dependent, noise-induced inversion of the effective potential $V_{\epsilon}^{(\text{eff})}$. This is also confirmed by the matrix continued-fraction treatment.

The paper is organized as follows: In Sec. II we present the Langevin and the corresponding Fokker-Planck equations for a CEL model of long-lived atoms. Section III is devoted to an approximate analysis of these equations. Moreover, we present the matrix continued-fraction treatment of the Fokker-Planck equation along with an outline of the electronic circuit. In Sec. IV we discuss the main results of the three approaches. Section V is a summary and conclusion.

II. LANGEVIN AND FOKKER-PLANCK EQUATIONS

The natural extension of the CEL Langevin equation for the relative phase difference between the two modes in the presence of Gaussian noise,¹⁴

$$\langle \epsilon(t)\epsilon(s) \rangle = \left[\frac{D}{\tau_c} \right] \exp \left[-\frac{|t-s|}{\tau_c} \right], \quad (2.1)$$

of noise intensity D and correlation time τ_c with zero mean,

$$\langle \epsilon(t) \rangle = 0, \quad (2.2)$$

is^{9,20,21}

$$\dot{\phi} = a + b \sin \phi + \epsilon(t) \sin \phi. \quad (2.3)$$

When we introduce

$$\dot{\epsilon} = - \left[\frac{1}{\tau_c} \right] \epsilon + F(t),$$

where

$$\langle F(t)F(s) \rangle = \left[\frac{2D}{\tau_c^2} \right] \delta(t-s),$$

the two-dimensional Fokker-Planck equation corresponding to Eq. (2.3) reads

$$\begin{aligned} \frac{\partial P}{\partial t} = & - \frac{\partial}{\partial \phi} \{ [a + (b + \epsilon) \sin \phi] P \} \\ & + \frac{1}{\tau_c} \frac{\partial (\epsilon P)}{\partial \epsilon} + \left[\frac{D}{\tau_c^2} \right] \frac{\partial^2 P}{\partial \epsilon^2}, \end{aligned} \quad (2.4)$$

where we impose periodic boundary conditions for ϕ ,

$$P(\phi + 2\pi, \epsilon) = P(\phi, \epsilon), \quad (2.5a)$$

and natural boundary conditions for ϵ ,

$$P(\phi, \epsilon \rightarrow \pm \infty) = 0. \quad (2.5b)$$

The Langevin equation (2.3) and the corresponding Fokker-Planck equation (2.4) are the starting points for the present paper.

III. STEADY-STATE DISTRIBUTIONS

In this section we discuss the three approaches used in the present paper to obtain the steady-state distributions $P_{SS}(\phi)$ of the colored-noise CEL. In order to gain deeper insight into the dependence of P_{SS} on the various parameters of interest such as the correlation time, we first present a linearized treatment of the Langevin equation (2.3). We then solve for the steady-state distribution P_{SS} of Eq. (2.4) and conclude by introducing an analog simulation of Eq. (2.3).

A. Approximate treatment

For small noise intensity, that is, for $D/b \ll 1$ and for small detuning $|a|/b \ll 1$, we can try the ansatz^{9,11}

$$\phi(t) \cong \pi + \arcsin(a/b) + \Delta(t), \quad (3.1)$$

where $|\Delta| \ll 1$. Thus Eq. (2.3) reduces to

$$\dot{\Delta} = -[\gamma + (\gamma/b)\epsilon(t)]\Delta - (a/b)\epsilon(t),$$

with the obvious solution

$$\begin{aligned} \Delta(t) = & \Delta_0 \exp \left[-\gamma t - \frac{\gamma}{b} \int_0^t dt' \epsilon(t') \right] \\ & - \frac{a}{b} \int_0^t dt' \epsilon(t') \exp \left[-\gamma(t-t') \right. \\ & \left. - \frac{\gamma}{b} \int_{t'}^t dt'' \epsilon(t'') \right]. \end{aligned} \quad (3.2)$$

Here, we have defined $\gamma \equiv (b^2 - a^2)^{1/2}$ and $\Delta_0 = \Delta(t=0)$. From Eq. (3.2) it is straightforward to evaluate the moments²² $\langle \Delta^j \rangle$ for $j=1$ and 2.

With the help of Eqs. (2.1) and (2.2) we can find from Eqs. (3.1) and (3.2) the center of gravity²³ $\langle \phi \rangle$ for the stationary distribution, at

$$\begin{aligned} \langle \phi \rangle \cong & \pi + \arcsin \left[\frac{a}{b} \right] + \langle \Delta \rangle \\ \cong & \pi + \arcsin \left[\frac{a}{b} \right] + (1 + \gamma \tau_c)^{-1} \left[\frac{a}{b} \right] \left[\frac{D}{b} \right], \end{aligned} \quad (3.3)$$

and the approximate width of P_{SS} is governed by

$$\sigma_{\text{app}}^2 = \langle \phi^2 \rangle - \langle \phi \rangle^2 \cong (1 + \gamma \tau_c)^{-1} \left[\frac{a}{b} \right]^2 \left[\frac{D}{\gamma} \right]. \quad (3.4)$$

The Gaussian,

$$P_{SS}^{(\text{app})}(\phi) = \frac{1}{\sqrt{2\pi}\sigma} \exp \left[-\frac{1}{2\sigma^2} (\phi - \langle \phi \rangle)^2 \right], \quad (3.5)$$

with $\langle \phi \rangle$ and σ given by Eqs. (3.3) and (3.4), thus represents the simplest approximation to the exact distribution P_{SS} calculated in Sec. III B.

From Eqs. (3.3), (3.4), and (3.5), we recognize that the noise color modifies the white noise ($\tau_c=0$) moments by the prefactor $(1 + \gamma \tau_c)^{-1}$, which signifies an enhancement of the noise-quenching characteristic of the CEL. We emphasize that this noise-color-enhanced quenching is an

entirely classical effect which may have applications to other systems. Nor does the quenching stem from the multiplicative nature of the noise in this particular application. For example, a similar result has been obtained¹⁸ for the standard phase-locked ring-laser Langevin equation¹¹

$$\dot{\phi} = a + b \sin\phi + \epsilon(t). \quad (3.6)$$

For this case, the width for the stationary distribution in the phase-locked region is approximately given¹⁸ by

$$\sigma_{\text{ring-laser}}^2 \cong (1 + \gamma\tau_c)^{-1} (D/\gamma), \quad (3.7)$$

which shows that the width, for this simpler case of additive noise, is governed by the same color prefactor.

The noise source $\epsilon(t)$ is multiplicative¹⁰ and so gives rise to a noise-induced asymmetry δ , which manifests itself as a separation of the center of gravity of P_{SS} and the location of its maximum ϕ_{max} , that is,

$$\delta = \langle \phi \rangle - \phi_{\text{max}}. \quad (3.8)$$

The expression for ϕ_{max} can be found by first deriving the corresponding expression for the white-noise case from the steady-state Fokker-Planck equation

$$0 = -\frac{d}{d\phi} \left[\left(a + b \sin\phi + \frac{D}{2} \sin(2\phi) \right) P_{\text{SS}} - D \frac{d}{d\phi} (\sin^2\phi P_{\text{SS}}) \right]. \quad (3.9)$$

According to Eqs. (3.4) and (3.5), the distribution P_{SS} is well localized for small noise $D/\gamma \ll 1$ and for small detuning $(a/b) \ll 1$. Hence, we can replace the periodic boundary conditions in ϕ with natural ones, that is, vanishing probability current. We thus find from Eq. (3.9) and the condition for an extremum of P_{SS} ,

$$0 = \frac{dP_{\text{SS}}}{d\phi} \Big|_{\phi=\phi_{\text{max}}} = \left(a + b \sin\phi_{\text{max}} - \frac{D}{2} \sin(2\phi_{\text{max}}) \right) P_{\text{SS}}.$$

It is easy to verify that this equation is satisfied by

$$\phi_{\text{max}}(\tau_c=0) = \pi + \arcsin(a/b) - (a/b)(D/b). \quad (3.10)$$

We find the corresponding colored-noise expression in the limit of small noise strength by replacing D by the effective diffusion constant of Hänggi,²⁴

$$D(\tau_c) \cong D \left[1 - \tau_c \left\langle \frac{d}{d\phi} (a + b \sin\phi) \right\rangle \right]^{-1}.$$

When we make use of Eq. (3.1) and neglect the noise-induced drift Δ , we find

$$D(\tau_c) \cong D(1 + \gamma\tau_c)^{-1},$$

which reduces Eq. (3.10) to

$$\phi_{\text{max}}(\tau_c) \cong \pi + \arcsin \left[\frac{a}{b} \right] - (1 + \gamma\tau_c)^{-1} \left[\frac{a}{b} \right] \left[\frac{D}{b} \right], \quad (3.11)$$

and the noise-induced asymmetry δ , from Eqs. (3.3) and (3.8), reads

$$\delta = \frac{2}{(1 + \gamma\tau_c)} \left[\frac{a}{b} \right] \left[\frac{D}{b} \right].$$

This asymmetry is obviously not contained in the Gaussian approximation, Eq. (3.5).

B. Exact treatment

We now turn to a formally exact solution of the Fokker-Planck equation (2.4) in steady state, in terms of infinite matrix continued fractions. The phase distribution as well as its lowest moments are discussed in this subsection.

1. Steady-state distribution

We start from the ansatz^{14,19}

$$P(t, \phi, \epsilon) = \frac{1}{\sqrt{2\pi}} \mathcal{H}_0(\epsilon) \sum_{m=0}^{\infty} \sum_{n=-\infty}^{\infty} \mathcal{S}_{m,n}(t) \mathcal{H}_m(\epsilon) e^{in\phi}, \quad (3.12)$$

where \mathcal{H}_m is given by

$$\mathcal{H}_m(\epsilon) = \mathcal{N}_m \exp \left[-\frac{\epsilon^2}{4(D/\tau_c)} \right] H_m \left[\frac{\epsilon}{\sqrt{2D/\tau_c}} \right].$$

The normalization factors \mathcal{N}_m are chosen to be $\mathcal{N}_m = [m! 2^m \sqrt{2\pi(D/\tau_c)}]^{-1/2}$, and the quantities H_m are the familiar Hermite polynomials. Since the probability density P is real, that is,

$$\mathcal{S}_{m,-n} = \mathcal{S}_{m,n}^*, \quad (3.13)$$

only the coefficients $\mathcal{S}_{m,n}$ for $n > 0$ must be determined. The ansatz Eq. (3.12) automatically satisfies the boundary conditions specified by Eqs. (2.5a) and (2.5b). We substitute Eq. (3.12) into Eq. (2.4) and project onto the coefficient $\mathcal{S}_{m,n}$ by making use of the orthogonality relations of the Hermite functions and the trigonometric functions. This procedure yields the following recurrence relation:

$$\begin{aligned} \dot{\mathcal{S}}_{m,n} = & -(ina + m/\tau_c) \mathcal{S}_{m,n} + \frac{nb}{2} \mathcal{S}_{m,n+1} \\ & + \frac{n}{2} \sqrt{D/\tau_c} (\sqrt{m+1} \mathcal{S}_{m+1,n+1} + \sqrt{m} \mathcal{S}_{m-1,n+1}) \\ & - \frac{nb}{2} \mathcal{S}_{m,n-1} - \frac{n}{2} \sqrt{D/\tau_c} (\sqrt{m+1} \mathcal{S}_{m+1,n-1} \\ & + \sqrt{m} \mathcal{S}_{m-1,n-1}), \end{aligned} \quad (3.14)$$

which can be cast into a three-term, vector-recurrence relation in two different ways as discussed in the next two subsections.

a. Vector-recurrence relation in n . When we define the m th component of the n th vector, \mathbf{S}_n , via

$$(\mathbf{S}_n)_m \equiv \mathcal{S}_{m,n}, \quad (3.15)$$

the recurrence relation, Eq. (3.14), now reads

$$\dot{\mathbf{S}}_n = \underline{A}_n \mathbf{S}_n + \underline{B}_n (\mathbf{S}_{n+1} - \mathbf{S}_{n-1}), \quad (3.16)$$

where we have introduced the matrices

$$(\underline{A}_n)_{m,m'} \equiv -(ina + m/\tau_c) \delta_{m,m'} \quad (3.17a)$$

and

$$(\underline{B}_n)_{m,m'} \equiv \frac{nb}{2} \delta_{m,m'} + \frac{n}{2} \sqrt{D/\tau_c} (\sqrt{m} \delta_{m-1,m'} + \sqrt{m+1} \delta_{m+1,m'}). \quad (3.17b)$$

In the steady state, the coefficients $\mathcal{S}_{m,n}^{(\infty)} \equiv \mathcal{S}_{m,n}(t \rightarrow \infty)$, that is, the vector $\mathbf{S}_n^{(\infty)}$ can be obtained from the iteration

$$\mathbf{S}_n^{(\infty)} = \underline{R}_n \mathbf{S}_{n-1}^{(\infty)}, \quad (3.18)$$

where \underline{R}_n is the infinite matrix continued fraction

$$\underline{R}_n = (\underline{A}_n + \underline{B}_n \underline{R}_{n+1})^{-1} \underline{B}_n. \quad (3.19)$$

From Eq. (3.14) we find for $n=0$ in the steady state,

$$0 = -(m/\tau_c) \mathcal{S}_{m,0}^{(\infty)},$$

and hence $\mathcal{S}_{m,0}^{(\infty)} = 0$ for $m \neq 0$. The coefficient $\mathcal{S}_{0,0}$ follows from the normalization of the probability distribution Eq. (3.12)

$$\begin{aligned} 1 &= \frac{1}{\sqrt{2\pi}} \int_{-\infty}^{\infty} d\epsilon \int_{-\pi}^{\pi} d\phi \mathcal{H}_0(\epsilon) \\ &\quad \times \sum_{m=0}^{\infty} \sum_{n=-\infty}^{\infty} \mathcal{S}_{m,n} \mathcal{H}_m(\epsilon) e^{in\phi} \\ &= \sqrt{2\pi} \mathcal{S}_{0,0}. \end{aligned}$$

Hence, the start vector \mathbf{S}_0 of the recurrence relation Eq. (3.18) reads

$$(\mathbf{S}_0)_m = \mathcal{S}_{m,0}^{(\infty)} = \frac{1}{\sqrt{2\pi}} \delta_{m,0}. \quad (3.20)$$

We now briefly outline the procedure for calculating the coefficients $\mathcal{S}_{m,n}^{(\infty)}$. Substituting the matrices \underline{A}_n and \underline{B}_n into Eq. (3.19) and using downward iteration¹⁴ yields the matrices \underline{R}_n and, in particular, \underline{R}_1 . The start vector \mathbf{S}_0 defined via Eq. (3.20) is then substituted into Eq. (3.18) together with \underline{R}_1 and we arrive at \mathbf{S}_1 . Continuing the iteration yields \mathbf{S}_n . The steady-state distribution $P_{SS} = P_{SS}(\phi)$ that follows from Eq. (3.12) then reads

$$\begin{aligned} P_{SS}(\phi) &= \frac{1}{\sqrt{2\pi}} \sum_{n=-\infty}^{\infty} \mathcal{S}_{0,n}^{(\infty)} e^{in\phi} \\ &= \frac{1}{\sqrt{2\pi}} \sum_{n=-\infty}^{\infty} (\mathbf{S}_n^{(\infty)})_0 e^{in\phi}. \end{aligned} \quad (3.21)$$

Hence in this approach P_{SS} is governed by the zeroth component of the n th vector \mathbf{S}_n . For a numerical evaluation of \underline{R}_n , Eq. (3.19), on the computer the infinite matrices \underline{A}_n and \underline{B}_n have to be truncated. We note that their dimension m determines via Eqs. (3.15) and (3.18) the number of Hermite functions included in Eq. (3.12),

that is, the influence of noise color. Figure 1(a) displays the probability curve $P_{SS}(\phi)$ obtained by this method for $a=0.3$, $D=1$, $\tau_c^{-1}=0.3$, and $b=1$.

b. Vector-recurrence relation in m . The recurrence relation Eq. (3.14) may be cast into a three-term vector-recurrence relation different from Eq. (3.16) by defining a new vector $\tilde{\mathbf{S}}_m$. In this case the n th component of the m th vector $\tilde{\mathbf{S}}_m$ follows from

$$(\tilde{\mathbf{S}}_m)_n \equiv \mathcal{S}_{m,n}. \quad (3.22)$$

The resulting vector-recurrence relation reads

$$\dot{\tilde{\mathbf{S}}}_m = \tilde{\underline{A}}_m \tilde{\mathbf{S}}_m + \tilde{\underline{B}}_m \tilde{\mathbf{S}}_{m+1} + \tilde{\underline{C}}_m \tilde{\mathbf{S}}_{m-1}, \quad (3.23)$$

where the matrices $\tilde{\underline{A}}_m$, $\tilde{\underline{B}}_m$, and $\tilde{\underline{C}}_m$ are given by

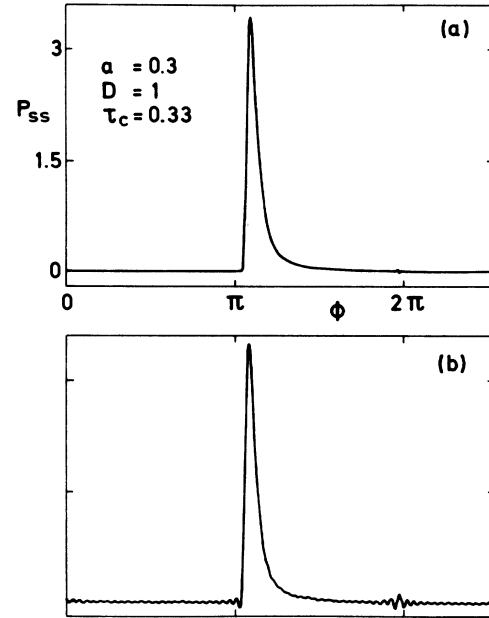


FIG. 1. Steady-state distributions $P_{SS} = P_{SS}(\phi)$ for the phase ϕ of a correlated emission laser governed by the Langevin equation (2.3) for the parameters $a=0.3$, $D=1$, $\tau_c^{-1}=0.3$, and $b=1$. The distribution displayed in (a) is obtained from the solution of the recurrence relation Eq. (3.16) for the vector \mathbf{S}_n . In contrast, the probability curve shown in (b) is the result of the three-term recurrence relation [Eq. (3.23)] for the vector $\tilde{\mathbf{S}}_m$. Here the number of Fourier coefficients, n_0 , taken into account in P_{SS} [Eq. (3.27)] is determined by the dimension of the matrix \underline{R}_m , [Eq. (3.26)]. It is too small and gives rise to the nonphysical oscillations shown in (b). In contrast, the more efficient method of (a) determines n_0 as the number of matrix inversions as indicated by Eqs. (3.18) and (3.19). Here the dimension of the matrix \underline{R}_n [Eq. (3.19)], denoted by m_0 , is governed by the number of Hermite functions, that is, by the amount of noise color, taken into account in Eq. (3.12). In (a) it suffices to have $m_0=40$ Hermite functions and $n_0=200$ Fourier coefficients, whereas for (b) we use $n_0=49$ and $m_0=48$.

$$(\tilde{A}_m)_{n,n'} \equiv - \left[ina + \frac{m}{\tau_c} \right] \delta_{m,n'} + \frac{nb}{2} (\delta_{n+1,n'} - \delta_{n-1,n'}), \quad (3.24a)$$

$$(\tilde{B}_m)_{n,n'} \equiv \frac{n}{2} \sqrt{D/\tau_c} \sqrt{m+1} (\delta_{n+1,n'} - \delta_{n-1,n'}), \quad (3.24b)$$

$$(\tilde{C}_m)_{n,n'} \equiv \frac{n}{2} \sqrt{D/\tau_c} \sqrt{m} (\delta_{n+1,n'} - \delta_{n-1,n'}). \quad (3.24c)$$

In steady state, this new vector-recurrence relation [Eq. (3.23)] can be solved in a way analogous to that of Eq. (3.16). The iteration

$$\tilde{\mathbf{S}}_m^{(\infty)} = \tilde{\mathbf{R}}_m \tilde{\mathbf{S}}_{m-1}^{(\infty)}, \quad (3.25)$$

with the matrix continued fraction

$$\tilde{\mathbf{R}}_m = -(\tilde{\mathbf{A}}_m + \tilde{\mathbf{B}}_m \tilde{\mathbf{R}}_{m+1})^{-1} \tilde{\mathbf{C}}_m \quad (3.26)$$

is then a solution of Eq. (3.23) in the steady state. Here the start vector \mathbf{S}_0 is determined by $(\tilde{\mathbf{A}}_0 + \tilde{\mathbf{B}}_0 \tilde{\mathbf{R}}_1) \tilde{\mathbf{S}}_0 = \mathbf{0}$ and $\mathcal{S}_{0,0} = (2\pi)^{-1/2}$, as described in detail in Refs. 18 and 19. The expression for the steady-state distribution then reads

$$P_{SS}(\phi) = \frac{1}{\sqrt{2\pi}} \sum_{n=-\infty}^{\infty} (\tilde{\mathbf{S}}_0^{(\infty)})_n e^{in\phi}. \quad (3.27)$$

In contrast to Eq. (3.21), it is now given by the n components of the $m=0$ vector $\tilde{\mathbf{S}}_0^{(\infty)}$.

This method has been used to evaluate again P_{SS} for parameters identical to those used in Fig. 1(a). The so-calculated distribution shown in Fig. 1(b) exhibits non-physical oscillations. Although both approaches are mathematically equivalent in the limits m and $|n| \rightarrow \infty$, the approach presented in Sec. III B 1 a is more suitable for the problem at hand. As a result of the noise quenching in the CEL, the steady-state distribution is highly peaked at a particular phase value. In order to obtain this property, many Fourier coefficients $\mathcal{S}_{0,n}^{(\infty)}$ must be included in the sum [Eq. (3.21) or (3.27)]. In the second approach, the number of Fourier coefficients, n_0 taken into account, that is, the number of components of the vector $\tilde{\mathbf{S}}_0^{(\infty)}$, is determined via Eq. (3.25) by the dimensions of the matrix $\tilde{\mathbf{R}}_m$, that is, via Eq. (3.26) by the dimension of the matrices $\tilde{\mathbf{A}}_m$, $\tilde{\mathbf{B}}_m$, and $\tilde{\mathbf{C}}_m$. Hence, in order to obtain good convergence for the sum in Eq. (3.27), huge matrices must be inverted over and over again. By contrast, the dimension of the matrices \mathbf{A}_n and \mathbf{B}_n to be inverted in the first approach is given by the number m_0 of Hermite functions to be included, as is apparent from Eq. (3.19). The number n_0 of Fourier coefficients then governs the number of iterations in Eq. (3.18).

2. Exact moments of P_{SS}

We conclude this subsection by evaluating the moments $\langle \phi \rangle$ and $\langle \phi^2 \rangle$ in steady state. The functions ϕ and ϕ^2 are nonperiodic. Hence the averages

$$\langle \phi \rangle \equiv \int_{0+\phi_0}^{2\pi+\phi_0} d\phi \phi P_{SS}(\phi) \quad (3.28a)$$

and

$$\langle \phi^2 \rangle \equiv \int_{0+\phi_0}^{2\pi+\phi_0} d\phi \phi^2 P_{SS}(\phi), \quad (3.28b)$$

using the periodic steady-state distribution, Eq. (3.21), depend on the starting point ϕ_0 of the integration region. Since the distributions $P_{SS} = P_{SS}(\phi)$ are strongly peaked in the neighborhood of $\phi = \pi$ and since the maximum of P_{SS} should be in the middle of the region, we choose $\phi_0 = 0$. When we substitute Eq. (3.21) into Eq. (3.28a) and use the relations

$$\int_0^{2\pi} d\phi \phi = \frac{(2\pi)^2}{2}$$

and

$$\int_0^{2\pi} d\phi \phi e^{in\phi} = \frac{2\pi}{in} \quad \text{for } n \neq 0,$$

together with Eqs. (3.13) and (3.20), we arrive for the choice of $\phi_0 = 0$ at

$$\langle \phi \rangle = \pi + \sqrt{2\pi} \sum_{n=1}^{\infty} \frac{2 \operatorname{Im}(\mathbf{S}_n^{(\infty)})_0}{n}. \quad (3.29)$$

For the second moment, Eq. (3.28b), we find, from

$$\int_0^{2\pi} d\phi \phi^2 = \frac{(2\pi)^3}{3}$$

and

$$\int_0^{2\pi} d\phi \phi^2 e^{in\phi} = \frac{(2\pi)^2}{in} + \frac{4\pi}{n^2} \quad \text{for } n \neq 0,$$

the following expression:

$$\begin{aligned} \langle \phi \rangle^2 &= \frac{(2\pi)^2}{3} + (2\pi)^{3/2} \sum_{n=1}^{\infty} \frac{2 \operatorname{Im}(\mathbf{S}_n^{(\infty)})_0}{n} \\ &\quad + \sqrt{2\pi} \sum_{n=1}^{\infty} \frac{4 \operatorname{Re}(\mathbf{S}_n^{(\infty)})_0}{n^2}. \end{aligned} \quad (3.30)$$

Equations (3.29) and (3.30) together allow us to evaluate the exact variance

$$\sigma_{\text{exact}}^2 \equiv \langle \phi^2 \rangle - \langle \phi \rangle^2. \quad (3.31)$$

The location of the maximum, ϕ_{max} , of the exact steady-state distribution P_{SS} can be found from the condition

$$0 = \frac{dP_{SS}}{d\phi} \Big|_{\phi=\phi_{\text{max}}} = \frac{1}{\sqrt{2\pi}} \sum_{n=-\infty}^{\infty} in (\mathbf{S}_0^{(\infty)})_n e^{in\phi} \Big|_{\phi=\phi_{\text{max}}}. \quad (3.32)$$

In Sec. IV we compare and contrast these expressions to the corresponding approximations of Sec. III A.

C. Electronic simulation

We now turn to the last of the three methods of obtaining the steady-state solution: the electronic simulation of the Langevin equation (2.3). The techniques for simulating periodic potentials with analog circuits have been

previously discussed,¹⁹ and here we use the same approach except for the following simple alterations: First, the hybrid analog-digital system for producing the spatially periodic force was replaced with an analog chip²⁵ which accomplishes the same task; and, second, an additional multiplier was used to implement the multiplicative noise. The voltages representing $\phi(t)$ were digitized into time series of approximately 4 000 000 points from which the stationary probability densities were assembled. In contrast to the simulation of the same system with additive noise described in Ref. 19, in the present case only the one-dimensional densities were measured. Our purpose is simply to demonstrate the phenomenon of noise quenching and the noise-color effects in this purely classical multiplicative system in accord with the predictions of Secs. III A and III B.

IV. DISCUSSION OF RESULTS

In this section we discuss the results obtained by the analog simulation of the Langevin equation (2.3), and the formally exact matrix continued-fraction treatment. Moreover, we compare the findings of the latter to the ones of the linearization scheme of Sec. III A.

The investigations of Ref. 9 concerned with the white-noise version of the central Langevin equation [Eq. (2.3)] have shown essentially three striking features of the steady-state distribution P_{SS} resulting from the multiplicative nature of the spontaneous-emission fluctuations of a CEL: (1) Within the locked region, that is, for $|a| < b$, the width of the distribution is dramatically reduced compared to the case of additive noise; (2) the probability density P_{SS} is highly asymmetric; and (3) the center of gravity of the distribution is shifted by the noise-induced drift.

These white-noise features prevail in the presence of noise color as shown by Figs. 2–8. Moreover, the analog simulation technique of Sec. III C reveals a novel effect shown in Fig. 2(a): The so-obtained steady-state probability density P_{SS} exhibits for $a = 0.25$, $D = b = 1$, and a correlation time $\tau_c = 0.1$, that is, for almost white noise, a long plateau in its right tail and a sharp break-off for small but positive values of the phase ϕ . When we increase the noise strength D , this plateau even develops into a second maximum of this distribution as is apparent from Fig. 3(d). This peak, located approximately at the unstable steady-state solution

$$\phi_{SS} = \arcsin \left[\frac{a}{b} \right]$$

of the deterministic equation of motion

$$\dot{\phi} = a + b \sin \phi, \quad (4.1)$$

is not present in the case of additive noise.^{9,14,18,19} Hence its origin lies in the multiplicative nature of the noise.²⁶ This intriguing phenomenon, making its appearance for large diffusion constants $D > b$ and small correlation times $\tau_c \ll 1/b$, is confirmed by the exact matrix continued-fraction treatment and can easily be understood by the following qualitative argument displayed in

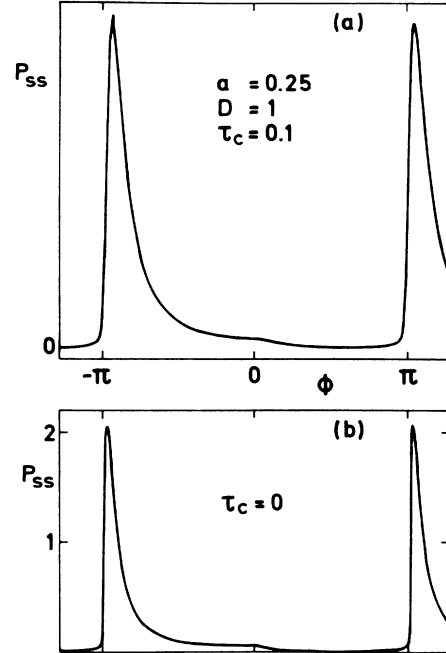


FIG. 2. Steady-state distribution $P_{SS} = P_{SS}(\phi)$ of the phase of a CEL for $a = 0.25$, $D = b = 1$, and $\tau_c = 0.1$ (quasiwhite noise) obtained from an analog simulation of the Langevin equation (2.3). The plateau in the long tail of P_{SS} and its sudden break-off at zero phase angle shown in (a) are confirmed by the matrix continued-fraction result of (b) made for the same values of parameters as in (a) except $\tau_c = 0$. The vertical axis in (a) is in arbitrary units.

Fig. 3 for $a = 1.0$ and $D = 1.5 > b = 1$. Equation (4.1) describes the overdamped motion of a particle of coordinate ϕ in the potential

$$V(\phi) = -a\phi + b \cos \phi \quad (4.2)$$

depicted in Fig. 3(a) for $a = b = 1$, that is, at the border between locked and unlocked solutions.^{11,14} In the presence of noise the qualitative steady-state probability P , depicted here by the dashed curve, exhibits a maximum at the minimum of V . The noise unlocks the system and P shows wings reaching into the regions outside of the potential minimum. The noise ϵ is Gaussian. Hence the quantity ϵ is distributed according to the function

$$P(\epsilon) \equiv \frac{1}{\sqrt{4\pi D}} \exp \left[-\frac{\epsilon^2}{4D} \right] \quad (4.3)$$

as shown in the insets of Figs. 3(b) and 3(c). According to Eq. (4.3), there exists a significant probability P for ϵ values such that $|\epsilon| > b$ provided $2\sqrt{D} > b$. As a result, the effective potential for Eq. (2.3),

$$V_{+\epsilon}^{(\text{eff})} = -a\phi + (b + \epsilon)\cos \phi, \quad (4.4)$$

shown in Fig. 3(b) by the solid line, has a deeper minimum than the one of Eq. (4.2) and additional probability P_ϵ , depicted qualitatively by a dashed curve, piles up at this coordinate. Due to the symmetry of the distribution (4.3), negative values of ϵ such that $b + \epsilon < 0$ also

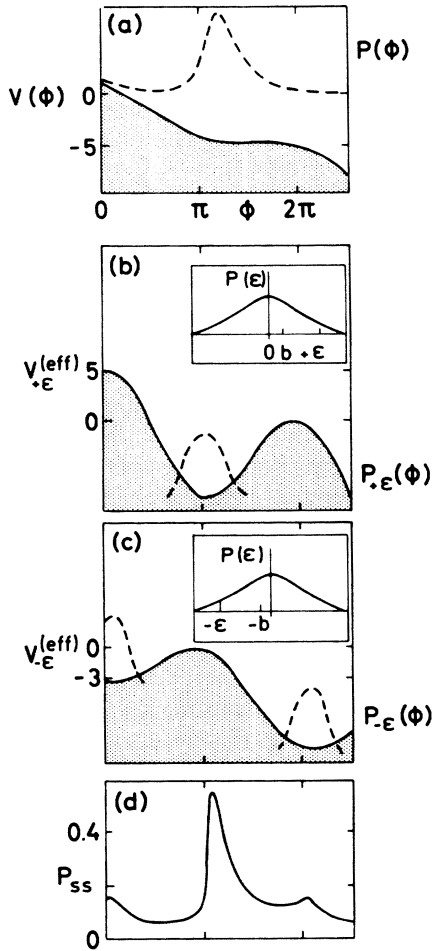


FIG. 3. Qualitative explanation of the second maximum in the steady-state distribution, P_{SS} , of the multiplicative noise process [Eq. (2.3)] for $a=1.0$, $D=1.5$, $b=1$, and $\tau_c=0$. In the presence of *additive* noise the steady-state distribution, shown qualitatively in (a) by the dashed line, exhibits a maximum at the location of the minimum of the potential, $V(\phi) = -a\phi + b \cos\phi$, depicted by the solid line. The presence of noise allows for running solutions and gives rise to the wings of the distribution in (a). The *multiplicative* noise ϵ , as defined via Eq. (2.1), obeys a Gaussian distribution of width D [Eq. (4.3)], shown by the insets of (b) and (c). Hence for $D \geq b$ there exists a significant probability for having a value of $\epsilon > b$. This creates an effective potential $V_{+\epsilon}^{(eff)}(\phi) = -a\phi + (b + \epsilon)\cos\phi$ of depth $b + \epsilon > b$, as indicated by the solid curve in (b). As a result, additional probability piles up at the location of the potential minimum. On the other hand, negative values of ϵ such that $\epsilon + b < 0$ are equally probable as indicated by the inset of (c). Consequently, the potential minimum of (b) turns into a maximum and the maximum into a minimum. Hence probability is collected at the location of the original potential maxima of (a) and (b) as indicated in (c) by the qualitative dashed curves. The exact steady-state distribution P_{SS} obtained from the continued-fraction treatment and shown in (d) is hence the modification of the distribution (a) due to the weighted average of the cases (b) and (c). Thus the *noise-induced inversion* of the potential is the origin of the second maximum in P_{SS} .

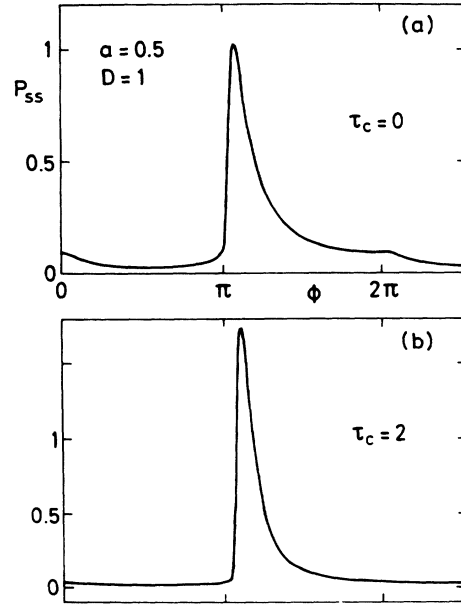


FIG. 4. Influence of noise color, that is, correlation time τ_c on the steady-state distribution P_{SS} [Eq. (3.21)], for $a=0.5$, $D=1.0$, and $b=1$. White noise, that is, $\tau_c=0$, shown in (a), displays a strong noise-induced asymmetry as well as the wide plateau reaching up to phase values of 2π . A correlation time of $\tau_c=2$, shown in (b), sharpens the phase distribution and thus reduces the asymmetry, while at the same time eliminating the plateau.

occur with the same probability leading to the potential

$$V_{-\epsilon}^{(eff)} = -a\phi - |\epsilon| - b|\cos\phi|, \tag{4.5}$$

as shown in Fig. 3(c). In this case the potential maxima of Figs. 3(a) and 3(b) turn into minima with accumulated probability $P_{-\epsilon}$. The total probability distribution P_{SS} , as given by the matrix continued-fraction treatment and shown in Fig. 3(d), is hence the sum of the curve shown in 3(a) and the distributions of 3(b) and 3(c) weighted according to the Gaussian distribution (4.3). The additional maximum at ϕ_{SS} of Eq. (4.1) arising from the noise-induced inversion of the potential $V_{-\epsilon}^{(eff)}$ [Eq. (4.5)] survives this averaging procedure.

The long-ranging plateau also appears within the locked region, that is, for $|a| < b$ as shown in Fig. 4(a) for the case of $a=0.5$, $D=1$, and $b=1$. It is, however, very sensitive to the correlation time τ_c . In Fig. 4(b) the value $\tau_c=2$ has made the plateau disappear as a result of the narrowing of P_{SS} . In addition, an increase in the correlation time tends to decrease the noise-induced asymmetry defined by the separation of the location of the maximum of the distribution, ϕ_{max} , and its center of gravity $\langle \phi \rangle$ [Eqs. (3.29) and (3.32)]. This is confirmed in more detail by Figs. 5(a) and 5(b) in which we show for parameters identical to the ones of Fig. 4 the noise-color-induced decrease of the asymmetry and the narrowing of the width of the distribution described by the second moment σ [Eq. (3.31)], respectively. This noise-color-induced shar-

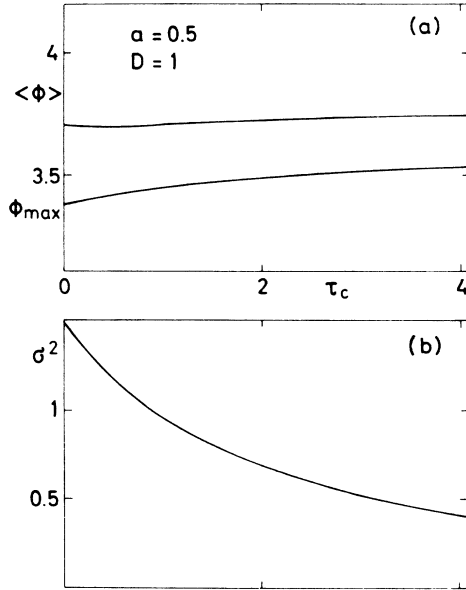


FIG. 5. Influence of noise color, that is, correlation time τ_c on the mean value $\langle \phi \rangle$, [Eq. (3.29)], on the location of the maximum, ϕ_{\max} [Eq. (3.32)] and on the variance $\sigma^2 = \langle \phi^2 \rangle - \langle \phi \rangle^2$ [Eq. (3.31)] of the steady-state distribution P_{SS} [Eq. (3.21)], displayed in (a) and (b), respectively. For increasing τ_c the maximum of P_{SS} , that is, ϕ_{\max} moves towards larger ϕ values, and so does $\langle \phi \rangle$. However, their separation $\delta = \langle \phi \rangle - \phi_{\max}$, caused by the noise-induced asymmetry, decreases. In addition, the distribution sharpens as expressed by σ^2 and the two examples of P_{SS} shown in Fig. 4. For (a) and (b) we have chosen identical parameters $a = 0.5$, $D = b = 1$.

pening of the distribution is illustrated in Fig. 6. Here we display for the parameters $a = 0.5$ and $D = b = 1$ the exact steady-state probability P_{SS} [Eq. (3.21)] in its dependence on noise correlation time τ_c . In Fig. 7 we compare and contrast the approximate and analytical curve $P_{SS}^{(app)}$, [Eq. (3.5)] shown by the dashed line to the corresponding

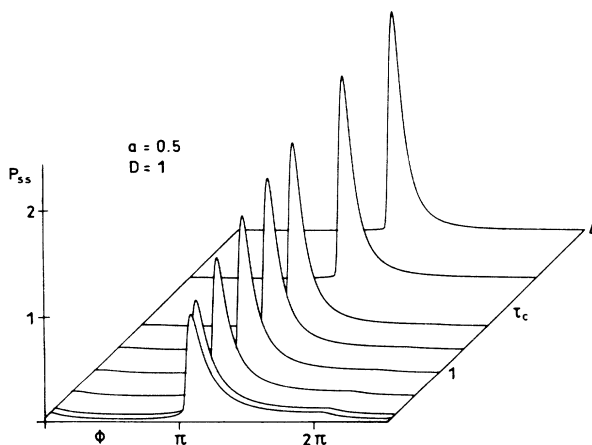


FIG. 6. Noise-color-induced narrowing of the steady-state distribution P_{SS} [Eq. (3.21)] of a colored-noise CEL for $a = 0.5$, $D = b = 1$. The plateau in the long tail of P_{SS} in the neighborhood of 2π displayed for white noise, that is, for $\tau_c = 0$ in the foreground of the picture, disappears for increasing τ_c and the distribution sharpens considerably.

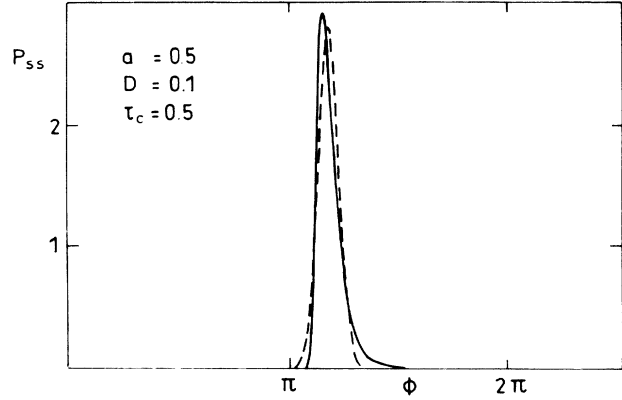


FIG. 7. Comparison between the exact steady-state distribution P_{SS} [Eq. (3.21)] obtained from matrix continued fractions and shown by the solid line and the approximate Gaussian expression, $P_{SS}^{(app)}$, Eq. (3.5) depicted by the dashed line for weak noise, $D = 0.1$. Here we have chosen $a = 0.5$, $\tau_c = 0.5$, and $b = 1$.

one of the exact matrix continued-fraction treatment, [Eq. (3.21)] in the weak-noise limit, that is, for $D = 0.1$. The other parameters are $a = 0.5$, $\tau_c = 0.5$, and $b = 1$. Figure 8 compares in more detail the approximate moments $\langle \phi \rangle$ and σ^2 , [Eqs. (3.3) and (3.4)] to the exact ones, Eqs. (3.29) and (3.31), together with the location of the maximum, ϕ_{\max} that is, Eq. (3.11) versus (3.32). Therefore, the linearization technique of Sec. III A provides a

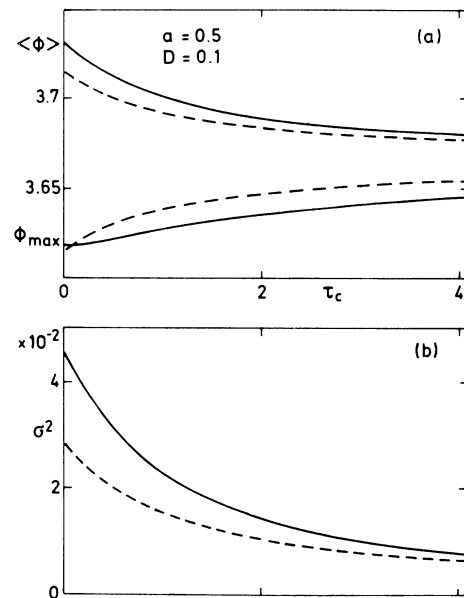


FIG. 8. Comparison between the approximate and analytical expressions for $\langle \phi \rangle$ [Eq. (3.3)], for ϕ_{\max} , [Eq. (3.11)], and for σ^2 [Eq. (3.4)], displayed by dashed lines, and their matrix continued-fraction counterparts, [Eqs. (3.29), (3.31), and (3.32)], shown by solid curves. Note that the approximate value for ϕ_{\max} shown by the dashed curve is not the maximum of $P_{SS}^{(app)}$, [Eq. (3.5)], which is $\langle \phi \rangle$, but is the expression, Eq. (3.11). The parameters identical for (a) and (b) are $a = 0.5$, $D = 0.1$, and $b = 1$.

good qualitative and quantitative description of the steady-state distribution of a CEL with colored noise.

V. SUMMARY AND CONCLUSIONS

In the present article we have investigated the influence of noise color on the steady-state distribution of the phase of the electromagnetic field in the CEL model of Eq. (2.3). In such a CEL device the spontaneous-emission noise enters in a multiplicative way giving rise to the celebrated noise quenching.⁵⁻⁹ We are therefore confronted with the topic of multiplicative colored noise in a periodic potential. We have approached this problem from three different directions: (1) By linearizing the nonlinear equation of motion, we find approximate and analytical expressions for P_{SS} and its moments, (2) an infinite matrix continued-fraction treatment allows a formally exact expressions for P_{SS} , and (3) an analog simulation of the underlying Langevin equation provides directly P_{SS} .

We have shown that only one of the two possible matrix continued-fraction solutions of the recurrence relation (3.14) corresponding to the Fokker-Planck equation, Eq. (2.4), reproduces in a most economical way the sharp peaks of the phase distribution, P_{SS} . With the help of

this technique we have extended the results of Ref. 9, which so far have dealt with weak white noise, to the case of large values of the diffusion constant D , as well as noise color. In the course of this work the analog simulation has brought to light another novel, noise-induced effect: an additional maximum of P_{SS} located approximately in the neighborhood of the unstable noise-free steady-state solution and caused by the multiplicative noise. This phenomenon is explained via a time-dependent, noise-induced inversion of the effective potential $V_{\epsilon}^{(eff)}$. Moreover, we have demonstrated that the quenching of spontaneous-emission fluctuations found in the white noise case is not only preserved in the case of colored noise but is even enhanced by an additional sharpening of the phase probability distribution.

ACKNOWLEDGMENTS

We are grateful to Th. Leiber and K. Vogel for several stimulating discussions. In particular, we thank M. O. Scully for introducing us to the concept of the CEL and for his continuous encouragement and support. This work was supported by the U.S. Office of Naval Research, No. N00014-88-K-0084 and by NATO, Grant No. 0770/85.

*Present address: Department of Physics, University of Wisconsin at Parkside, Kenosha, WI 53141.

¹For the role of quantum noise in *passive* interferometers, see C. M. Caves, Phys. Rev. D **23**, 1693 (1981).

²For a review on gravitational wave detection using Michelson interferometers, see, for example, W. Winkler, G. Wagner, and G. Leuchs in *Fundamentals of Quantum Optics II*, Vol. 282 of *Lecture Notes in Physics*, edited by F. Ehlotzky (Springer-Verlag, Berlin, 1987).

³M. O. Scully and J. Gea-Banacloche, Phys. Rev. A **34**, 4043 (1986).

⁴For a review on ring-laser gyroscopes, see W. W. Chow, J. Gea-Banacloche, J. M. Pedrotti, V. E. Sanders, W. Schleich, and M. O. Scully, Rev. Mod. Phys. **57**, 61 (1985).

⁵M. O. Scully, Phys. Rev. A **35**, 452 (1987); J. Krause and M. O. Scully, *ibid.* **36**, 1771 (1987).

⁶M. O. Scully, Phys. Rev. Lett. **55**, 2802 (1985).

⁷M. O. Scully and M. S. Zubairy, Phys. Rev. A **35**, 752 (1987); J. Bergou, M. Orszag, and M. O. Scully, *ibid.* **38**, 768 (1988); S. Swain, J. Mod. Opt. **35**, 1 (1988); **35**, 103 (1988).

⁸For experimental realizations of CEL devices, see P. Toschek and J. Hall, in *XV International Conference on Quantum Electronics Technical Digest Series* (Optical Society of America, Washington, D. C., 1987), Vol. 21, p. 102; M. P. Winters and J. Hall, in *XVI International Conference on Quantum Electronics Technical Digest Series* (Optical Society of America, Washington, D. C., 1988), Vol. 22; M. Ohtsu and K.-Y. Liou, Appl. Phys. Lett. **52**, 10 (1988).

⁹For a geometrical derivation of the Langevin equation governing the CEL, see W. Schleich and M. O. Scully, Phys. Rev. A **37**, 1261 (1988). A rigorous derivation of this equation starting from the quantum Langevin equations of the two CEL modes of Ref. 6 using a semiclassical amplitude-phase representation can be found in W. Schleich, M. O. Scully, and H.-

G. von Garssen, Phys. Rev. A **37**, 3010 (1988).

¹⁰A. Schenzle and H. Brand, Phys. Rev. A **20**, 1628 (1979); R. Graham and A. Schenzle, *ibid.* **25**, 1731 (1982); H. Brand, A. Schenzle, and G. Schröder, *ibid.* **25**, 2324 (1982); W. Horsthemke and R. Lefever, *Noise Induced Transitions, Theory and Applications in Physics, Chemistry and Biology* (Springer-Verlag, Berlin, 1984).

¹¹See, for example, H. Haken, H. Saueremann, Ch. Schmid, and H. D. Vollmer, Z. Phys. **206**, 369 (1967); W. W. Chow, M. O. Scully, and E. W. van Stryland, Opt. Commun. **15**, 6 (1975); J. D. Cresser, W. H. Louisell, P. Meystre, W. Schleich, and M. O. Scully, Phys. Rev. A **25**, 2214 (1982).

¹²M. O. Scully, G. Süßmann, and C. Benkert, Phys. Rev. Lett. **60**, 1014 (1988).

¹³M. Sargent, M. O. Scully, and W. E. Lamb, *Laser Physics* (Addison-Wesley, Reading, MA 1974).

¹⁴H. Risken, *The Fokker-Planck Equation, Methods of Solution and Application*, Vol. 18 of *Springer Series in Synergetics*, edited by H. Haken (Springer-Verlag, Berlin, 1984).

¹⁵For a treatment of white pump fluctuations, see Ref. 14 and, in particular, P. Jung, Th. Leiber, and H. Risken, Z. Phys. B **66**, 397 (1987). The case of colored noise can be found in P. Jung and H. Risken, Phys. Lett. **103A**, 38 (1984), or in Th. Leiber, P. Jung, and H. Risken, Z. Phys. B **68**, 123 (1987).

¹⁶A similar equation also describes the phase of the electromagnetic field in a two-photon CEL. See, for example, M. O. Scully, K. Wodkiewicz, M. S. Zubairy, J. Bergou, N. Lu, and J. Meyer ter Vehn, Phys. Rev. Lett. **60**, 1832 (1988); see also C. Benkert, W. Schleich, and M. O. Scully, in *Atomic Physics*, edited by S. Haroche, J. C. Gay, and G. Grynberg (World Scientific, Singapore, 1989).

¹⁷For a review on possible approaches towards colored noise, see the relevant articles in *Noise in Nonlinear Dynamical Systems*, edited by F. Moss and P. V. E. McClintock (Cambridge

University Press, Cambridge, England, 1989).

- ¹⁸Noise-color-induced narrowing of the distribution function of a phase-locked laser has been noted for the case of additive noise by K. Vogel, Diplomarbeit, Universität Ulm, Federal Republic of Germany, 1986; K. Vogel, Th. Leiber, H. Risken, P. Hänggi, and W. Schleich, *Phys. Rev. A* **35**, 4882 (1987); and in the Kubo oscillator by R. Kubo, *J. Math. Phys.* **4**, 174 (1963).
- ¹⁹K. Vogel, H. Risken, W. Schleich, M. James, F. Moss, and P. V. E. McClintock, *Phys. Rev. A* **35**, 463 (1987); K. Vogel, H. Risken, W. Schleich, M. James, F. Moss, R. Manella, and P. V. E. McClintock, *J. Appl. Phys.* **62**, 721 (1987).
- ²⁰For reasons related to the construction of the electronic circuit the phase ϕ used throughout this article differs from the phase of the earlier CEL work (Ref. 9) by a phase shift π , which does not introduce any change in the physics. Moreover, the factor $\frac{1}{2}$ in the argument of the sine function in front of the noise in the two-mode CEL, as shown in the previous CEL references, has been omitted for simplicity. From the linearization ansatz, Eq. (3.1), we recognize that for this parameter regime, that is, for $|a| \ll b$ and $D \ll b$, it essentially redefines the noise intensity. Note, however, that the phase of the electric field of the two-photon CEL (Ref. 16) obeys Eq. (2.3).
- ²¹For a discussion of this equation in the case of white noise, see

I. I. Fedchenia and N. A. Usova, *Z. Phys. B* **50**, 263 (1983); **52**, 69 (1983).

- ²²It is well known (Ref. 10) that linearization of a Langevin equation with multiplicative noise yielding an equation such as $\dot{\Theta} = (-b + \epsilon)\Theta$ leads to divergent higher moments,

$$\begin{aligned} \langle \Theta^n \rangle &= \left\langle \exp \left[n \left(-bt + \int_0^t dt' \epsilon(t') \right) \right] \right\rangle \\ &= \exp[-n(b - nD)t], \end{aligned}$$

where, for simplicity, we have assumed white noise. Obviously, this expression diverges for moments of order $n > b/D$. In this work, however, we confine the discussion to the first two moments only, which, over the range of parameters considered, do not diverge.

- ²³In Eq. (3.6) of Ref. 9 the minus sign should be replaced by a plus sign.
- ²⁴P. Hänggi, *Z. Phys. B* **31**, 407 (1978); P. Hänggi, T. J. Mroczkowski, F. Moss, and P. V. E. McClintock, *Phys. Rev. A* **32**, 695 (1985); P. Hänggi, Ref. 17.
- ²⁵Analog Devices Model No. AD639.
- ²⁶A similar effect, that is, stabilization by multiplicative noise, has been discussed in the context of the bistable potential by R. Graham and A. Schenzle, *Phys. Rev. A* **26**, 1676 (1982).

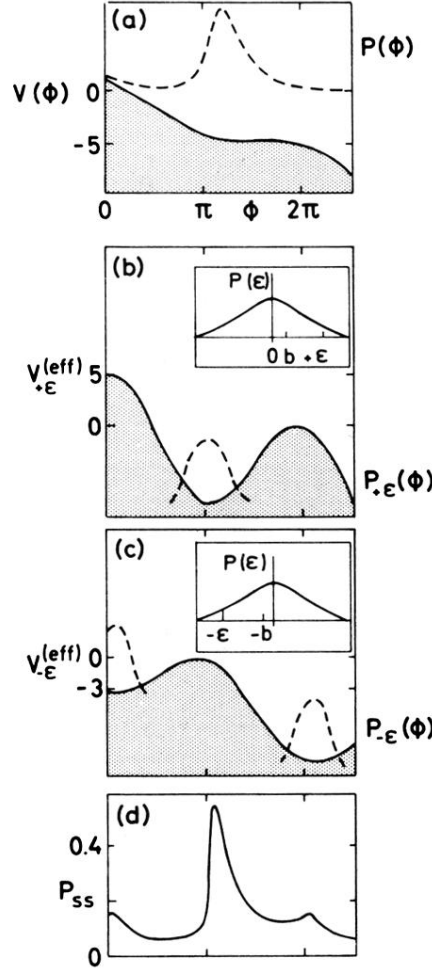


FIG. 3. Qualitative explanation of the second maximum in the steady-state distribution, P_{ss} , of the multiplicative noise process [Eq. (2.3)] for $a = 1.0$, $D = 1.5$, $b = 1$, and $\tau_c = 0$. In the presence of *additive* noise the steady-state distribution, shown qualitatively in (a) by the dashed line, exhibits a maximum at the location of the minimum of the potential, $V(\phi) = -a\phi + b \cos\phi$, depicted by the solid line. The presence of noise allows for running solutions and gives rise to the wings of the distribution in (a). The *multiplicative* noise ϵ , as defined via Eq. (2.1), obeys a Gaussian distribution of width D [Eq. (4.3)], shown by the insets of (b) and (c). Hence for $D \geq b$ there exists a significant probability for having a value of $\epsilon > b$. This creates an effective potential $V_{+\epsilon}^{(eff)}(\phi) = -a\phi + (b + \epsilon)\cos\phi$ of depth $b + \epsilon > b$, as indicated by the solid curve in (b). As a result, additional probability piles up at the location of the potential minimum. On the other hand, negative values of ϵ such that $\epsilon + b < 0$ are equally probable as indicated by the inset of (c). Consequently, the potential minimum of (b) turns into a maximum and the maximum into a minimum. Hence probability is collected at the location of the original potential maxima of (a) and (b) as indicated in (c) by the qualitative dashed curves. The exact steady-state distribution P_{ss} obtained from the continued-fraction treatment and shown in (d) is hence the modification of the distribution (a) due to the weighted average of the cases (b) and (c). Thus the *noise-induced inversion* of the potential is the origin of the second maximum in P_{ss} .